Robotica (2014) volume 32, pp. 823–834. © Cambridge University Press 2013
doi:10.1017/S0263574713001173

Three-dimensional swimming robotic fish with slide-block structure: design and realization

Yongnan Jia* and Long Wang

Intelligent Control Laboratory, College of Engineering, Peking University, Beijing 100871, P. R. China

(Accepted November 17, 2013. First published online: December 16, 2013)

SUMMARY

This paper focuses on the mechanism design of a slide-block structure and its application on a biomimetic modular robotic fish for three-dimensional swimming. First, as a barycenter-adjustor, the slide-block structure is integrated into a mechanical design of a robotic fish, which is constructed by a control module, a driving module, and a fan-shaped caudal fin. The three-dimensional locomotion of robotic fish is decomposed into two-dimensional locomotion in horizontal plane and ascent–descent locomotion in vertical plane. Both the kinematics of the horizontal swim and the dynamics of the ascent–descent swim are analyzed by the curve fitting method. Finally, experimental results validate the three-dimensional swimming capability of the robotic fish. Furthermore, the impact of two design parameters on the swimming capability of the robotic fish is discussed by the experimental method. The experimental results confirm that the robotic fish with one driving module and a fan-shaped low-aspect-ratio caudal foil can produce higher propulsive speed than other parameter combinations.

KEYWORDS: Autonomous underwater vehicles; Biomimetic robots; Mechatronic systems.

1. Introduction

Fish tends to be adaptive and optimized to their environments.[1,2] In order to endow modern underwater vehicles with favorable propulsive efficiency, maneuverability, and low-noise performance like real fish, more and more engineers have been involved in the study of robotic fish. Existing studies concerning robotic fish mainly focus on kinematic and hydrodynamic analysis of ichthyologic propulsion mechanisms,[3–5] biologically inspired behavior design of robotic fish,[6–10] and cooperation of multi-robots.[11,12]

Most of these studies only consider two-dimensional locomotion, which limits the activity areas of robotic fish to water surface. For the requirement of seabed resource detection, salvage, military detection, undersea operation, oceanic supervision, aquatic life-form observation, pollution search, and other practical applications, the significance of the study on three-dimensional swim has gradually risen up. As one of the distinct difficulties on three-dimensional motion, the control problem of ascent–descent locomotion is seldom explored except the few ones.[9,10,13–15] We have summarized these literatures into two categories.

One category is inspired by the aquatic organisms relying on pectoral fins for ascent and descent. There are two main approaches. One approach takes into account the effect obtained through the adjustment of attack angle of pectoral fins.[9,13] In this case, the robotic fish is expected to have paired pectoral fins and be initialized with a definite forward swimming velocity. Another approach is realized on a remote-control robotic fish, which performs ascent–descent motions by manipulating a pair of two-degree-of-freedom pectoral fins.[14] However, the relevant model parameters of pectoral fins, such as lag angles between heaving and pitching motions, are difficult to be optimized since complex hydrodynamics arise from the two-dimensional locomotion control of pectoral fins.

The second category uses natural forces of buoyancy and gravity to generate the torques necessary for ascend and descend. The movement principle that utilizes spatial shift of the system's center of

* Corresponding author. E-mail:ynjia@pku.edu.cn

gravity with respect to its center of buoyancy was first introduced by Baz and Gumusel in 1987,[16] and was used to control robot arms in underwater environment.[17,18] By virtue of efficient drives, accurate payload position, and fast speed response, the same principle has also been used to a structure called center-of-gravity controller[10] or barycenter-adjustor,[15] which is incorporated into a multi-link robotic fish wrapped in a gas-filled, rippled rubber tube.[15] However, such robotic fish has very poor capability on pressure resistance and cannot implement the underwater task well.

The main contributions of our work in this paper are the mechanism design of a slide-block structure and its application on a biomimetic modular robotic fish for three-dimensional swim. The robotic fish is proposed by incorporating simple control parameters and pressure resistance capability of considerable depth. The robotic fish is constructed by a control module, a driving module, and a caudal fin. A slide-block structure, embedded inside the control module, is presented as a barycenter-adjustor, cooperating with driving modules and caudal fin to endow robotic fish with the capability of three-dimensional locomotion. The three-dimensional swim of the robotic fish is decomposed into two-dimensional locomotion in horizontal plane and ascent–decent locomotion in vertical plane. The two-dimensional locomotion is achieved by the joint angle control of caudal fin, while the ascent–descent locomotion is realized by regulating the slide-block structure with the assistance of caudal fin. We give the motion control of horizontal swim and ascent–descent swim and analyze their swimming effect by the curve fitting method. Finally, experimental results validate the three-dimensional swimming capability of the robotic fish. Besides, two design parameters impacting the swimming capability of the robotic fish are discussed. One is the number of driving modules, and the other is the combination of the aspect ratio and the rigidity of caudal foil. Experimental results give a set of optimized parameters.

The rest of this paper is organized as follows. In Section 2, a slide-block structure applied on a modular robotic fish is elaborately explicated. Section 3 describes the three-dimensional swim analysis of robotic fish, including kinematic analysis of horizontal swim and dynamic analysis of ascent–descent swim. Section 4 presents experimental results of three-dimensional swimming and optimizes design parameters. Finally, the paper is concluded in section 5.

2. Slide-Block Structure and Its Application on a Modular Robotic Fish

Many scientists are trying to develop a robotic fish with excellent three-dimensional swimming capability. In order to design such specific robotic fish, the main challenge here is how to use the natural forces of buoyancy and gravity to generate the torques necessary to achieve ascent–descent movements of the robotic fish driven by caudal fin. We do not consider the case in which robotic fish emerges from water when it swims in a three-dimensional environment. Thus, the buoyancy center of the robotic fish is fixed. Then ascent–descent motions can only be realized by changing the barycenter of robotic fish. In order to endow robotic fish with a simple yet effective seal structure, the barycenter-adjustor mechanism is expected to be fixed inside the fish body for monolithic waterproof design. The difficulty is how to design such a smart barycenter-adjustor mechanism in a limited space. Besides, the total weight of robotic fish should be as small as possible to a certain extent for the sake of effective control of ascent–descent motions and low energy costs of three-dimensional motions. In this paper the authors have constructed such a mechanism called the slide-block structure and have utilized it for the control of ascent–descent motions successfully.

Figure 1(a) shows the interior assembly of the slide-block structure, which consists of a front plank, a back plank, a slippery bar, a lead screw, two drive gears, a slide-block, and a motor. When a control signal is added to the motor, the slide-block moves forward or backward along the lead screw depending on the transmission of two drive gears. That is to say, the displacement angle of the motor is transformed into the linear displacement of the slide-block. As a result, the robotic fish rises or sinks in the underwater environment.

Figure 2 shows the mechanism structure of a robotic fish. There are two kinds of functional modules, the control module and the driving module. Each functional module is sealed independently by an O-ring. Thus, the failure of one module has no influence on the other. A flapping fan-shaped caudal fin is properly chosen for robotic fish. We will further compare our caudal fin with a common caudal fin in section 4.2.2. An overview of the interior layout of control module is presented in Fig. 1(b).

https://doi.org/10.1017/S0263574713001173 Published online by Cambridge University Press

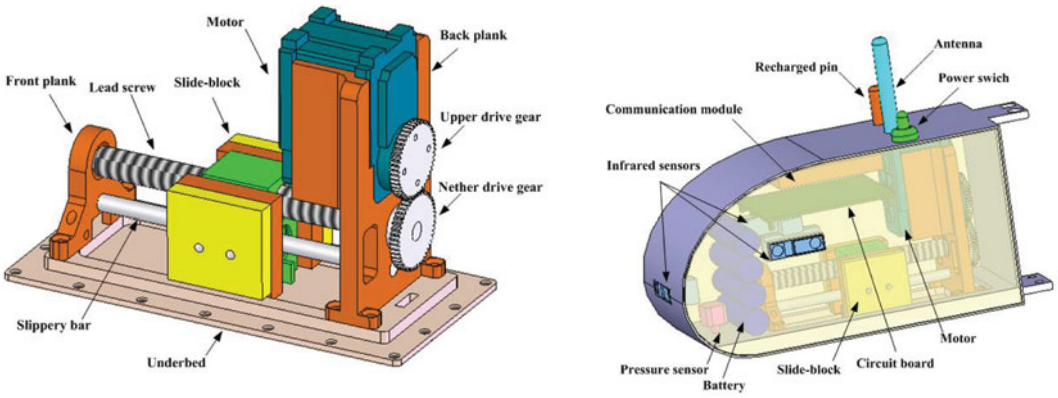

(a) Slide-block structure. (b) Control module.

Fig. 1. (Colour online) Interior assembly of control module with slide-block structure.

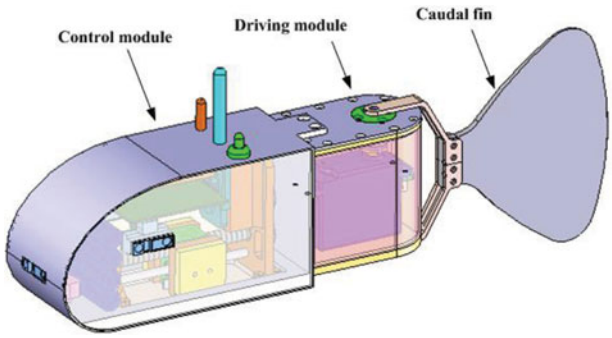

Fig. 2. (Colour online) Prototype of the robotic fish.

There are three infrared sensors and a pressure sensor equipped in the control module for collision avoidance and real-time depth control. An analog-to-digital converter is adopted to transform sensor signals. Two infrared sensors are embedded in the side covers with the position of fish eyes, and the third one is adorned in the position of fish mouth. The pressure sensor is fixed in the bottom of the frame and its probe can get in touch with external environment. The left infrared sensor is used to detect distances between robotic fish and obstacle on its left side, and the right infrared sensor is used to measure distances between robotic fish and obstacle on its right side, while the front infrared sensor is used to detect distance between robotic fish and obstacle in its front. The pressure sensor is utilized to measure distance from robotic fish to the bottom of the swimming pool. For the sake of convenient maintenance and further exploitation, the slide-block structure is installed on the base of the control module. Here the base is screwed to supporting frame and sealed with an O-ring. The design of the driving module is based on the predecessor of a previous study.[14] Table I summarizes the specification of robotic fish.

3. Three-Dimensional Swim Analysis

For easy implementation, the three-dimensional swim of robotic fish is recomposed into two-dimensional locomotion in horizontal plane and ascent–decent locomotion in vertical plane. The two-dimensional locomotion is achieved by the joint angle control of caudal fin, while the ascent–descent locomotion is realized by means of the coordination between the slide-block structure and the flapping caudal fin.

3.1. Kinematic analysis of horizontal swim

Due to the uncertainty and complexity of underwater environment, the model built by theory analysis methods may not be commonly suitable for the study of robotic fish. Therefore, the experimental

https://doi.org/10.1017/S0263574713001173 Published online by Cambridge University Press

Table I. Specification of robotic fish.

Item	Value
Weight	1.5 kg
Number of driving module	1
Power supply	5 V
Driving mode	Servomotor
Wireless communication frequency	444 Hz
Microcontroller	AT91SAM7A3
Dimensions (L × W × H)	411 × 72 × 95 mm

Table II. Forward speed v_F (cm/s) with different oscillatory frequencies f_c (Hz).

v_f	$f_c = 0.2$	$f_c = 0.36$	$f_c = 0.48$	$f_c = 0.6$	$f_c = 0.72$	$f_c = 0.84$	$f_c = 0.96$	$f_c = 1.08$	$f_c = 1.25$
$N = 1$	5.71884	9.23018	10.13048	12.24138	11.94536	15.57772	17.5	17.41642	27.0936
$N = 2$	5.73351	7.78886	11.46702	14.34527	12.13094	10.85074	14.77833	25.57545	23.0179
$N = 3$	6.37101	8.08767	10.15543	10.15543	9.245	14.98217	14.95116	19.85778	27.53778
$N = 4$	4.92611	10.31527	11.46702	12.55916	13.89891	18.08457	17.19902	22.16749	26.14882
$N = 5$	5.85222	7.38916	9.828	10.15543	13.24138	11.01511	14.98217	23.5794	25.65186
$N = 6$	5.08767	10.43769	11.01511	12.78772	10.85074	13.773	17.15653	18.75806	29.7612
$N = 7$	7.78886	8.08767	9.828	10.15543	13.26395	14.98217	17.24138	20.46036	27.5456
$N = 8$	3.05222	7.15543	11.46702	10.15543	11.46702	12.31527	18.13094	23.23641	28.08314
$N = 9$	5.1151	9.85222	12.31527	12.78772	9.828	16.47628	19.70899	19.85778	26.18263
$N = 10$	4.362	8.08767	10.42418	11.01511	12.31527	16.5227	17.76134	20.46036	25.9775

method has caused more attention of scholars because of its extensive adaptability and practicability, which is adopted for kinematic analysis of horizontal swim in this paper.

Fish swims either by body and caudal fin (BCF) or by median and paired fin. In this paper, the robotic fish functions under the BCF swimming pattern. To facilitate physical implementation, the motion control of the flexible fan-shaped caudal fin is described by[14]

$$\theta_c(t) = \phi_c + A_c \sin(2\pi f_c t). \tag{1}$$

Let the subscript c denote the flexible fan-shaped caudal fin, θ_c denote the angular position at the time t, ϕ_c denote the angular offset, A_c denote the amplitude, and f_c denote the oscillatory frequency. The average linear speed at the time t depends on the oscillatory frequency f_c and the amplitude A_c. The turning capability of the robotic fish is related with the angular offset ϕ_c, the oscillatory frequency f_c, and the amplitude A_c. Here $f_c \in (0, 1.5)$ Hz, $A_c \in (0, 65)^\circ$, and $A_c + \phi_c \in (-80^\circ, 80^\circ)$, which are set according to the performance of the hardware system.

3.1.1. ***Propulsive swim analysis***. The output thrust of the robotic fish mainly depends on the oscillation of the fan-shaped caudal fin. Here we consider the oscillatory frequency of the caudal fin as the only control parameter to adjust the swimming speed. Given $A_c = 20^\circ$ and $\phi_c = 0^\circ$, let robotic fish swim with 10 different frequencies f_c. Experimental results show that the trajectory of the robotic fish is nearly a straight line. For example, robotic fish swims nearly along the purple dotted line on condition that $f_c = 0.48$ Hz (see Fig. 3).

Test platform can output robotic fish's forward speed v_f every 40 ms. We randomly choose 10 forward speeds of robotic fish under each frequency; especially, when $f_c = 0$ Hz, we have $v_f = 0$ cm/s. The forward speeds of the robotic fish with other nine frequencies are shown in Table II. N denotes the number. Let v_F be the average value of 10 forward speeds under each frequency. We show the relationship between the average linear speed v_F and the oscillatory frequency f_c in the upper part of Fig. 4(a).

Since the swimming viscous drag and the mechanical thrust of fish are both nonlinear with their speeds,[19] it is obvious that the relationship between the average linear speeds of the robotic fish and

https://doi.org/10.1017/S0263574713001173 Published online by Cambridge University Press

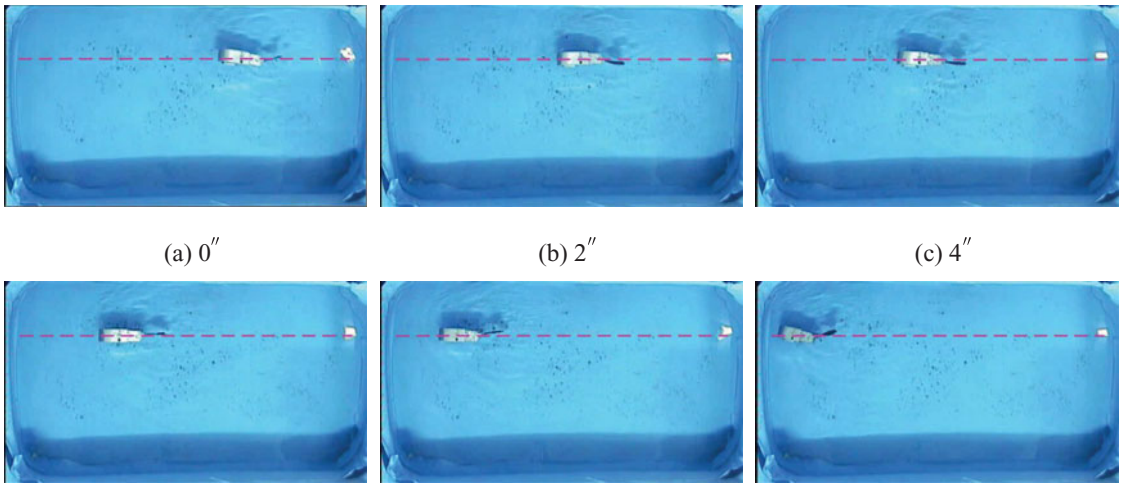

(a) 0″ (b) 2″ (c) 4″

(d) 6″ (e) 8″ (f) 10″

Fig. 3. (Colour online) Propulsive swim tests of robotic fish. $\phi_c = 0°$, $A_c = 20°$, and $f_c = 0.48$ Hz.

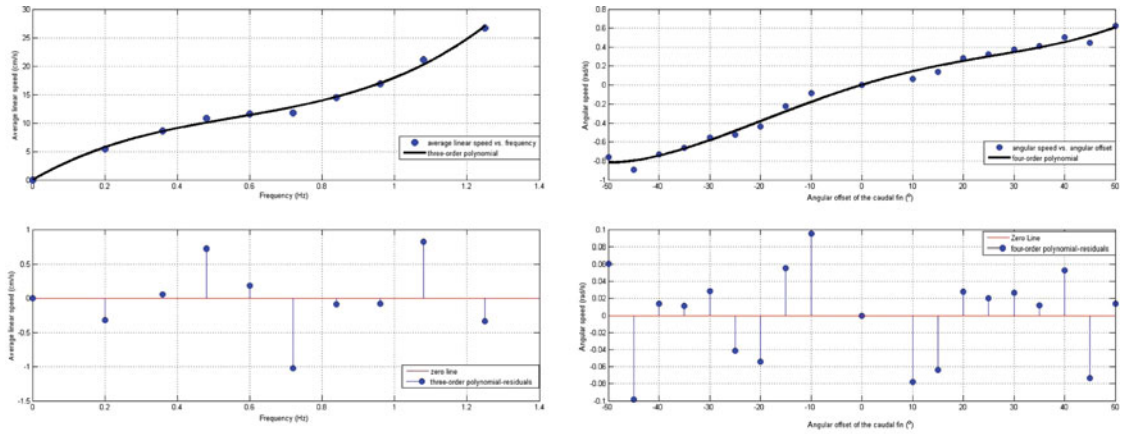

(a) (b)

Fig. 4. (Colour online) Data analysis by curve fitting method. (a) Average linear speed of forward swim with different oscillatory frequencies ($\phi_c = 0$, $A_c = 20°$). (b) Angular velocity with different angular offsets of caudal fin ($f_c = 0.6$ Hz, $A_c = 20°$).

the oscillatory frequencies of its tail fin is nonlinear. Considering a compromise between calculated quantity and accurate expression, we use the curve fitting method to draw their relationship by the third-order polynomial with a satisfied goodness of fit (R^2: 0.9952):

$$v_F = 26.57 f_c^3 - 45.14 f_c^2 + 36.54 f_c. \tag{2}$$

Figure 4(a) shows the proposed fitting curve and the residuals.

3.1.2. ***Maneuverability swim analysis***. Here the maneuverability of robotic fish refers to turning capability. We mainly discuss that how angular offset of the caudal fin affects the turning swim. Given $A_c = 20°$ and $f_c = 0.48$ Hz, let robotic fish swim with different angular offset ϕ_c and track its swimming trajectory. Robotic fish does a nearly circular swimming under each angular offset. For example, robotic fish swims along the purple dotted circular curve shown in Fig. 5. At the same time, we record the cost time T. Then we can compute out the relative angular velocity by $\omega_F = 2\pi/T$. Repeat the above process under different angular offsets and note the experimental data in Table III. Similarly, we utilize the curve fitting method to obtain approximate nonlinear law between the angular

https://doi.org/10.1017/S0263574713001173 Published online by Cambridge University Press

Table III. Maneuverability swim data on the relationship between $1/T$ (Hz) and ϕ_c (°); especially when $\phi_c = 0°$, one gets $1/T = 0$ Hz.

ϕ_c	−50	−45	−40	−35	−30	−25	−20	−15	−10
$1/T$	0.0992	0.0713	0.0804	0.0650	0.0596	0.0513	0.0450	0.0221	0.0105
ϕ_c	10	15	20	25	30	35	40	45	50
$1/T$	–0.0133	–0.0354	–0.0693	–0.0836	–0.0881	–0.1051	–0.1164	–0.1424	–0.1206

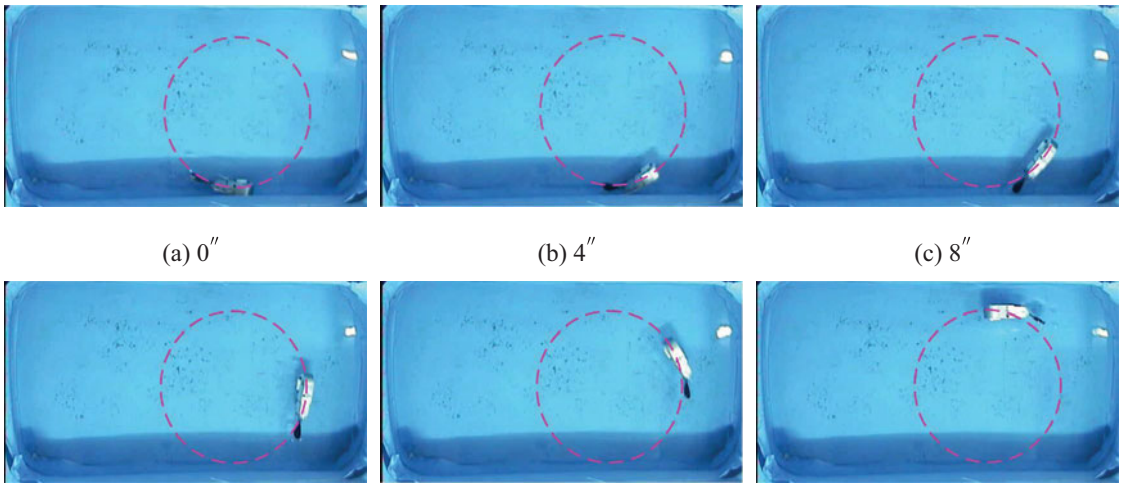

(a) 0″ (b) 4″ (c) 8″

(d) 13″ (e) 19″ (f) 23″

Fig. 5. (Colour online) Maneuverability swim tests of robotic fish. $\phi_c = 30°$, $A_c = 20°$, and $f_c = 0.48$ Hz.

speed ω_F and the angular offset ϕ_c with a satisfied goodness of fit (R^2: 0.9882) as follows:

$$\omega_F = 5.529 \times 10^{-8}\phi_c^4 - 7.695 \times 10^{-7}\phi_c^3 - 0.00018\phi_c^2 + 0.0162\phi_c. \tag{3}$$

Figure 4(b) shows the proposed fitting curve and the residuals. Suppose the initial heading of the robotic fish is ϕ_0, then the yaw angle (heading angle) of the robotic fish can be computed by

$$\phi_F = \phi_0 + \int_0^t \omega_F dt = \phi_0 + \int_0^t (5.529 \times 10^{-8}\phi_c^4 - 7.695 \times 10^{-7}\phi_c^3 - 0.00018\phi_c^2 + 0.0162\phi_c)dt. \tag{4}$$

3.2. Dynamic analysis of ascent–descent swim

For the conveniency of description, three coordinate frames are built as shown in Fig. 6(a). $O - XYZ$ denotes the earth frame, and $O_f - X_f Y_f Z_f$ denotes the body-fixed frame for fish. The longitudinal axis of fish body is the X_f-axis, the transverse axis of fish body is the Y_f-axis direction, and the direction of Z_f-axis is decided by the right-hand rule. $O_f(x_f, y_f, z_f)$ denotes the position coordinate of robotic fish in the earth frame. Here we consider that the swimming direction of the robotic fish is the same with X_f-axis. The yaw angle of the robotic fish can be expressed by the angle between the projection line of X_f-axis on the horizontal plane (XOY plane) and the X-axis of the earth frame (shown in Fig. 6(d)), while the pitch angle of the robotic fish can be expressed by the angle between the projection line of X_f-axis on the vertical plane (XOZ plane) and the X-axis of the earth frame (shown in Fig. 6(b)). If the angle is obtained by the counterclockwise rotation from X-axis to X_f-axis projection line, the angle is positive. $O_c - X_c Y_c Z_c$ denotes the body frame fixed in the caudal fin. The caudal fin body-fixed frame just rotates around the Z_c-axis and the rotational angle θ_c affects the horizontal swim of the robotic fish. Besides, $O_c(x_c, 0, 0)$ locates at the position of the pivot in the fish body-fixed frame. The counterclockwise direction of angle is positive. Therefore, the pose of the robotic fish can be described by five parameters: x_f, y_f, z_f, ϕ_F, and ϕ_V.

https://doi.org/10.1017/S0263574713001173 Published online by Cambridge University Press

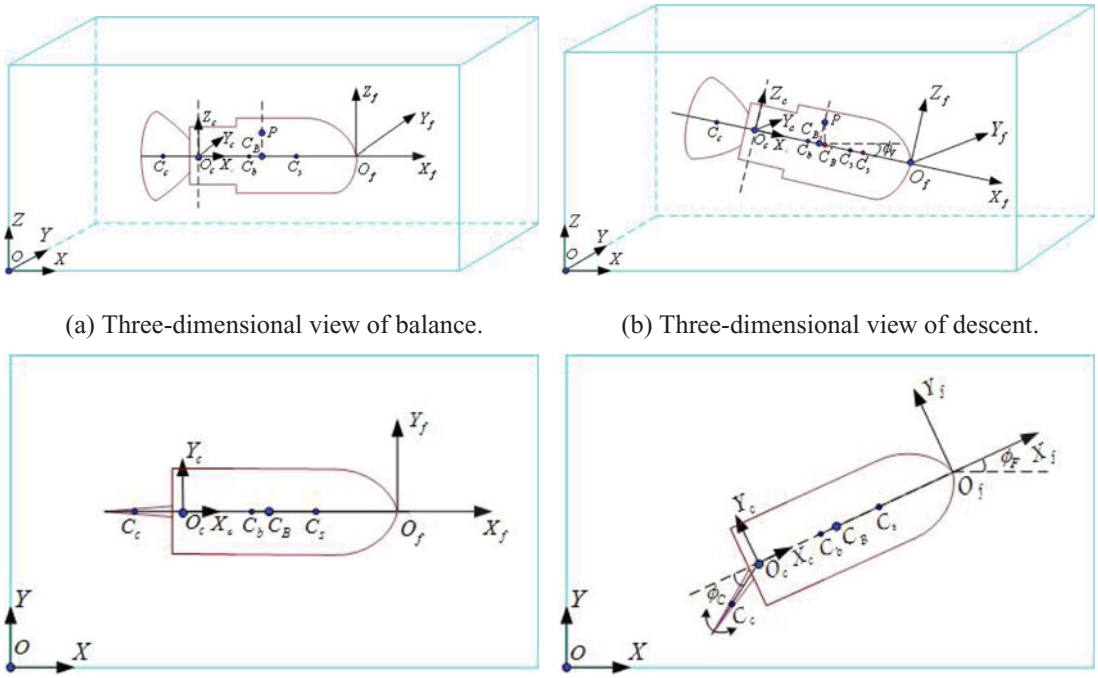

(a) Three-dimensional view of balance.

(b) Three-dimensional view of descent.

(c) Top view of forward movement.

(d) Top view of turning movement.

Fig. 6. (Colour online) Modeling analysis.

In Fig. 6, $C_c(L_c, 0, 0)$, $C_s(x_s, 0, 0)$, $C_b(x_b, 0, 0)$, and $C_B(x_B, 0, 0)$ are respectively the barycenter of the caudal fin, the slide-block, the fish body without slide-block, and the whole fish body. L_c is the distance between the barycenter of the caudal fin and the point O_c. m denotes the weight of the slide-block, M_1 denotes the weight of the robotic fish without the slide-block, M_2 denotes the weight of the caudal fin. Besides, the buoyancy center $P(x_B, 0, h)$ of the robotic fish is just above C_B to keep the robotic fish stabile vertically. When the slide-block is located at a proper position $C_s(x_s, 0, 0)$, the robotic fish balances horizontally (shown in Fig. 6(a)). According to the leverage theory, the relationship can be expressed as

$$mx_s + M_1x_b + M_2(x_c + L_c) = (m + M_1 + M_2)x_B. \tag{5}$$

In case the slide-block moves forward at a distance $X = x_s^{'} - x_s$ from the initial position C_s to the terminal position $C_s^{'}(x_s^{'}, 0, 0)$ (shown in Fig. 6(b)), the barycenter of the whole fish body accordingly moves from C_B to $C_B^{'}$, and other barycenters remain unchanged. Then the relationship similar to Eq. (5) can be shown as

$$mx_s^{'} + M_1x_b + M_2(x_c + L_c) = (m + M_1 + M_2)x_B^{'}. \tag{6}$$

As a consequence, the robotic fish can be stabilized only when $C_B^{'}$ is lowered vertically beneath P, then we have

$$\tan\phi_V = \frac{x_B - x_B^{'}}{h}. \tag{7}$$

Since $\phi_V \in (-\frac{\pi}{2}, \frac{\pi}{2})$, we can obtain the pitch angle ϕ_V of robotic fish as

$$\phi_V = -\arctan\frac{mX}{h(m + M_1 + M_2)}. \tag{8}$$

https://doi.org/10.1017/S0263574713001173 Published online by Cambridge University Press

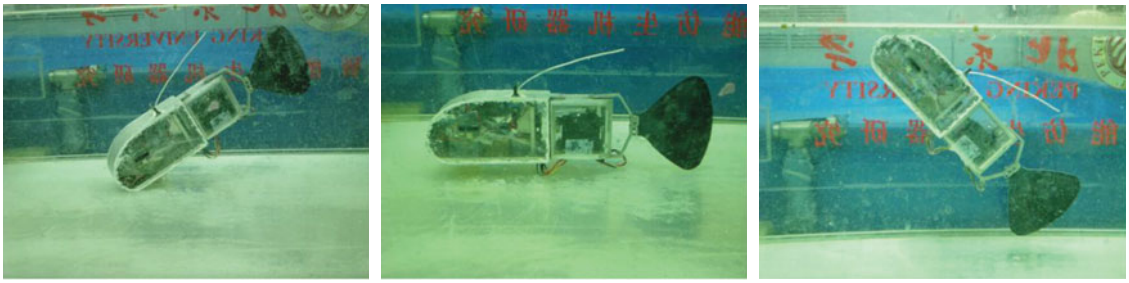

(a) Descent motion. (b) Horizontal motion. (c) Ascent motion.

Fig. 7. (Colour online) The ascent–descent swimming motions of robotic fish.

Here the weight of the slide-block is constant. On the assumption that the robotic fish swims in an ideal situation without considering the disturbance and resistance factors, the relationship between the vertical orientation angle ϕ_V of the robotic fish and the displacement X of the slide-block is obtained as Eq. (8).

Here ascent–descent experiments are actualized to probe the influence of displacement of the slide-block structure on the effect of ascent and descent motions. When the initial forward swimming speed is zero, the robotic fish is able to keep horizontal in equilibrium on condition that the slide-block is at a proper position as shown in Fig. 7(b). In experiment one, the slide-block glides to the most front part (near the head). Consequently, the robotic fish engenders a nose-down gesture and produces a maximal descent angle as shown in Fig. 7(a). Similarly, in experiment two, the slide-block structure glides to the most rear part (near the tail). Then the barycenter of the robotic fish moves backward correspondingly. In this case, the robotic fish engenders a nose-up gesture and produces a maximal ascent angle as shown in Fig. 7(c).

We have obtained that $h = 3$ mm, $m = 200$ g, $M_1 = 1086$ g, and $M_2 = 10$ g. Besides, when the robotic fish is horizontally balanced, the position of the slide-block is about 12 mm far from the forefront of lead screw. According to formula (8), the maximal descent angle of the robotic fish is

$$\phi_V = -\arctan\frac{200 \times 12}{3(200 + 1086 + 10)} = -31.7^\circ, \tag{9}$$

and the maximal ascent angle is approximately

$$\phi_V = -\arctan\frac{200 \times (-18)}{3(200 + 1086 + 10)} = 42.8^\circ. \tag{10}$$

It is obvious that the maximal descent angle and the maximal ascent angle computed by formula (8) coincide with the proposed experimental results shown in Figs. 7(a) and (c). Thus, to a certain extent, model (8) can draw the ascent–descent motions of robotic fish.

3.3. Three-dimensional swim analysis

In order to simplify the problem, the classical approach is to assign the amplitude A_c with a constant value, and use the oscillatory frequency f_c as the only parameter to adjust the forward swimming speed. Furthermore, the turning swim capability in horizontal is mainly drawn by the angular offset ϕ_c. Therefore, the three-dimensional swimming orientation of the robotic fish can be expressed by the complex of ϕ_F and ϕ_V. Therefore, the three-dimensional locomotion state of the robotic fish can be scaled by three variables, which are the oscillatory frequency f_c, the angular offsets ϕ_c, and the slide-block displacement X. Furthermore, the behavior of the robotic fish in three-dimensional environments can be expressed as a combination of five typical swimming gaits, that is, descent motion, ascent motion, left-turning motion, right-turning motion, and straight-going motion.

https://doi.org/10.1017/S0263574713001173 Published online by Cambridge University Press

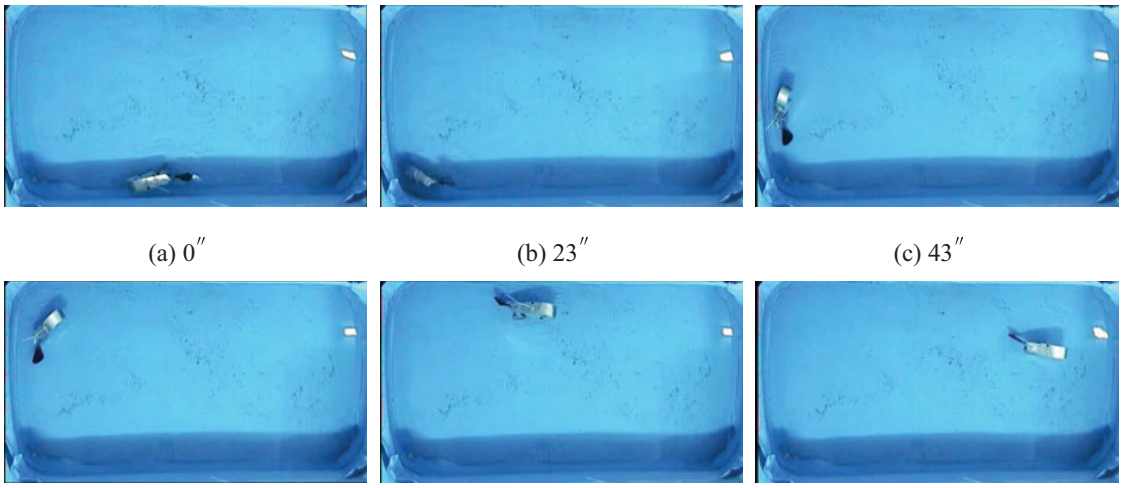

(a) 0″ (b) 23″ (c) 43″

(d) 52″ (e) 1′19″ (f) 1′51″

Fig. 8. (Colour online) A sequence of three-dimensional swimming.

4. Experimental Results

4.1. Three-dimensional locomotion tests

Figure 8 shows the sequence of three-dimensional swimming of robotic fish. The robotic fish starts to swim with descent motion. When robotic fish swims to the bottom, it switches the swimming mode to ascent motion. After rising to the water surface, the robotic fish stays stably in the horizontal plane. Experimental results indicate that the three-dimensional swimming motion of the robotic fish is realized, and the slide-block structure can adjust velocity and motion trajectory. Furthermore, the maneuverability of the robotic fish is verified. At some high velocity, the robotic fish can even turn 180° within a span that is a robotic fish body length.

4.2. Design parameters' discussion on swimming effect

4.2.1. Number of driving modules. According to the proportion participating in the undulation motion to the whole fish body, fish under BCF locomotion is divided into four categories, that is, anguilliform mode, subcarangiform mode, carangiform mode, and thunniform mode.[20] The four swimming modes can be formed by the modular robotic fish using various combinations of driving modules. More driving modules bring a larger undulation proportion to the fish body length, causing faster drop in propulsion efficiency, such as the anguilliform mode. Therefore, lesser number of driving modules are preferential to be adopted for the imitation of carangiform or thunniform mode.

In order to validate this argument, we take two robotic fish with distinct configurations for a comparison. Lighthill[4] has given the undulatory motion of carangiform robotic fish, which takes the form of a traveling wave as

$$y_{\text{body}}(x,t) = (c_1 x + c_2 x^2) sin(kx + 2\pi f t), \tag{11}$$

where y_{body} represents the transverse displacement of fish body, x denotes the displacement along the main axis, k indicates the body wave number ($k = 2\pi/\lambda$), λ is the body wave length, c_1 is the linear wave amplitude envelope, c_2 is the quadratic wave amplitude envelope, and f is the wave frequency. As illustrated in Figs. 9(a) and (b), one robotic fish is equipped with two driving modules and its body traveling wave can be expressed as

$$y_{\text{body}}(x,t) = (0.17x^2 - 4.68x)\sin(kx + 2\pi f t) \tag{12}$$

by the curve fitting method.[9] Similarly, the other is equipped with one driving module and its body traveling wave is given by

$$y_{\text{body}}(x,t) = (0.009x^2 - 0.208x)\sin(kx + 2\pi f t). \tag{13}$$

https://doi.org/10.1017/S0263574713001173 Published online by Cambridge University Press

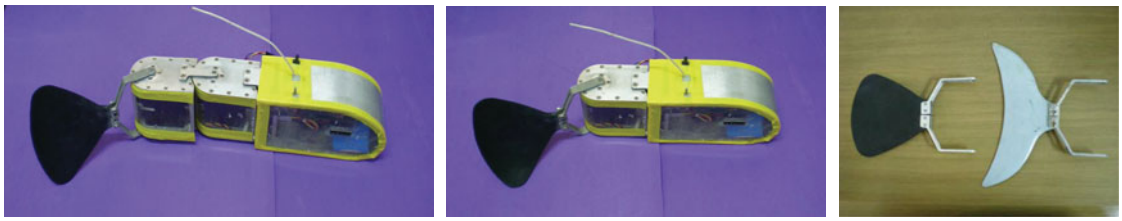

(a) (b) (c)

Fig. 9. (Colour online) Different configurations of robotic fish. (a) Robotic fish with two driving modules. (b) Robotic fish with one driving module. (c) Two types of caudal foils. The former caudal foil is a flexible, fan-shaped caudal foil (area: 11, 026 mm^2, aspect ratio:1.83) and made of rubber, while the latter one is a stiff, crescent-shaped caudal foil (area: 7095.9 mm^2, aspect ratio: 4.07) and is made of hardwood.

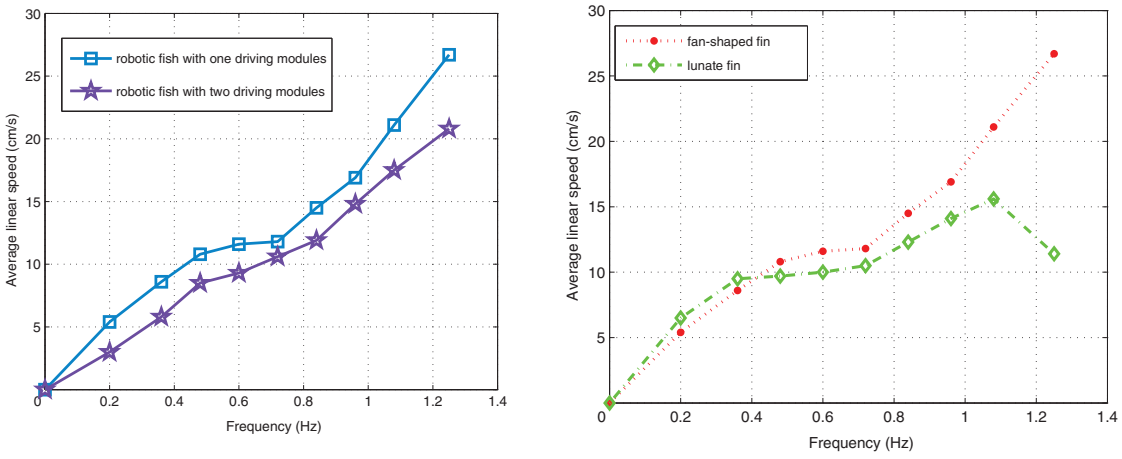

(a) (b)

Fig. 10. (Colour online) Analysis of experimental data. (a) The average linear speed of two robotic fish each equipped with one and two driving modules with different oscillatory frequencies. (b) Average linear speed of two robotic fish equipped with different caudal fins under different oscillatory frequencies at $A_c = 20^\circ$. Experimental results prove that the fan-shaped caudal foil of low aspect ratio leads to higher efficiency for miniature underwater vehicles than the crescent-shaped caudal foil of high aspect ratio.

Suppose $A_c = 20^\circ$, then Fig. 10(a) exhibits the relationship between the average linear speed and the oscillatory frequency of each robotic fish and further testifies that one driving module induces a higher speed to robotic fish. Hence, only one driving module is applied and the robotic fish swims just by swaying the caudal foil.

4.2.2. Combination of aspect ratio and rigidity of caudal foil. The aspect ratio of the caudal foil AR is defined as

$$AR = \frac{L^2}{S}, \tag{14}$$

where L is the span of the foil and S is the area of the foil surface. It has been demonstrated that the foil with a higher aspect ratio actually performs better.[21] Nevertheless, some new points of view are obtained by means of plentiful experiments in this paper, which can be considered as a revision to the above conclusion. Figure 9(c) shows two caudal foils, that is, a flexible, fan-shaped caudal foil of low aspect ratio and a stiff, crescent-shaped caudal foil of high aspect ratio. Each caudal foil is assembled to test the average linear speed of robotic fish under the identical oscillatory frequency in two-dimensional space. Here the oscillatory amplitude is constant.

It can be seen in Fig. 10(b) that the robotic fish equipped with crescent-shaped caudal foil moves faster at the frequencies ranging from 0 to 0.4 Hz than the robotic fish equipped with fan-shaped caudal foil. However, when the frequency lies in the interval of 0.4 to 1.4 Hz, the speed of the latter

https://doi.org/10.1017/S0263574713001173 Published online by Cambridge University Press

robotic fish exceeds that of the former one; especially, when the frequency is above 1.1 Hz, the speed of the former robotic fish begins to decrease. In contrast, the speed curve of the latter robotic fish shows an almost exactly linear increase with the oscillatory frequency in an aggrandized span. Experimental results show that the fan-shaped caudal foil induces higher speed especially under the frequency higher than 0.4 Hz.

A flexible caudal foil of low aspect ratio can keep balance well and show fine maneuverability for miniature underwater vehicles, while a stiff caudal foil of high aspect ratio is more appropriate for large-scale underwater vehicles.[22] Moreover, the stiff caudal foil of high aspect ratio is somewhat subject to the limited capability of maintaining balance. Therefore, although a stiff, crescent-shaped caudal foil is preferentially chosen in the existent projects, the aforementioned effort tells that the flexible, fan-shaped flapping caudal foil of lower aspect ratio produces higher speed and better maneuverability for small autonomous underwater vehicles (AUVs) such as the modular robotic fish.

5. Conclusions

We have developed a biomimetic modular robotic fish with slide-block structure. The function of the slide-block structure is especially emphasized because it endows the robotic fish with three-dimensional swimming capability. The three-dimensional swim of the robotic fish is decomposed into two-dimensional locomotion in horizontal plane and ascent–descent locomotion in vertical plane. Both the kinematics of the horizontal swim and the dynamics of the ascent–descent swim are analyzed by the curve fitting method. Experimental results have shown feasibility and effectiveness of the proposed motion control method. Furthermore, experimental results have also confirmed that the robotic fish with one driving module and a fan-shaped low-aspect-ratio caudal foil can produce higher propulsive speed than other parameter combinations.

Acknowledgments

The authors would like to thank Guangming Xie and Qining Wang of Peking University for their helpful discussions and valuable assistance.

References

1. G. V. Lauder and K. F. Liem, "The evolution and interrelationships of the actinopterygian fishes," *Bull. Mus. Comp. Zool.* **150**, 95–197 (1983).
2. J. S. Nelson, *Fishes of the World,* 4th ed. (John Wiley, New York, NY, 2006).
3. D. Barrett, M. Grosenbaugh and M. Triantafyllou, "The Optimal Control of a Flexible Hull Robotic Undersea Vehicle Propelled by an Oscillating Foil," *Proceedings of the IEEE Symposium on Autonomous Underwater Vehicle Technology* (1996) pp. 1–9.
4. M. J. Lighthill, "Note on the swimming of slender fish," *J. Fluid Mech.* **9**, 305–317 (1960).
5. T. Yao-Tsu Wu, "Hydromechanics of swimming propulsion. Part 3. Swimming and optimum movements of slender fish with side fins," *J. Fluid Mech.* **46**, 545–568 (1971).
6. R. Mason and J. Burdick, "Experiments in Carangiform Robotic Fish Locomotion," *Proceedings of the IEEE International Conference on Robotics and Automation*, Vol. 1 (2000) pp. 428–435.
7. K. McIsaac and J. Ostrowski, "A Geometric Approach to Anguilliform Locomotion: Modeling of an Underwater eel Robot," *Proceedings of the IEEE International Conference on Robotics and Automation*, Vol. 4 (1999) pp. 2843–2848.
8. N. Kato and M. Furushima, "Pectoral Fin Model for Manuever of Underwater Vehicles," *Proceedings of the IEEE Symposium on Autonomous Underwater Vehicle Technology* (1996) pp. 49–56.
9. J. Yu, L. Wang and M. Tan, "A Framework for Biomimetic Robot Fish's Design and its Realization," *Proceedings of the 2005 American Control Conference* (2005) pp. 1593–1598.
10. H. Hu, J. Liu, I. Dukes and G. Francis, "Design of 3D Swimming Patterns for Autonomous Robotic Fish," *IEEE/RSJ International Conference on Intelligent Robots and Systems*, Vols. 1–12 (2006) pp. 2406–2411.
11. S. Kalantar and U. R. Zimmer, "Scale-Adaptive Polygonal Formations of Submersible Vehicles and Tracking Isocontours," *IEEE/RSJ International Conference on Intelligent Robots and Systems*, Vols. 1–3 (2008) pp. 3146–3151.
12. D. Zhang, L. Wang and J. Yu, "Coordinated Control of Two Biomimetic Robotic Fish in Pushing-Object Task," *IET Control Theory Appl.* **3**, 281C293 (2009).
13. K. A. Morgansen, B. I. Triplett and D. J. Klein, "Geometric methods for modeling and control of free-swimming fin-actuated underwater vehicles," *IEEE Trans. Robot.* **23**, 1184–1199 (2007).
14. Y. Hu, L. Wang, W. Zhao, Q. Wang and L. Zhang, "Modular Design and Motion Control of Reconfigurable Robotic Fish," *IEEE Conference on Decision and Control*, Vols. 1–14 (2007) pp. 5156–5161.

15. C. Zhou, Z. Cao, S. Wang and M. Tan, "The Posture Control and 3D Locomotion Implementation of Biomimetic Robot Fish," *IEEE/RSJ International Conference on Intelligent Robots and Systems*, Vols. 1–12 (2006) pp. 5406–5411.
16. L. Gumusel, Buoyancy Gravity-Powered Underwater Robot *Master's thesis*, Department of Mechanical Engineering, The Catholic University of America, Washington, DC, 1987.
17. A. Baz and L. Gumusel, "Optimum design of a buoyancy and gravity-driven underwater robot," *J. Robot. Syst.* **13**(7), 461–473 (1996).
18. A. Baz and L. Gumusel, "Experimental and theoretical evaluation of the buoyancy and gravity-driven underwater robots," *Robotica* **13**(3), 273–286 (1995).
19. M. Sfakiotakis, D. M. Lane and J. B. C. Davies, "Review of fish swimming modes for aquatic locomotion," *IEEE J. Ocean. Eng.* **24**, 237–252 (1999).
20. C. C. Lindsey, "Form, function and locomotory habits in fish," *Fish Physiol.* **7**, 1C100 (1978).
21. K. H. Low and C. W. Chong, "Parametric study of the swimming performance of a fish robot propelled by a flexible caudal fin," *Bioinspir. Biomim.* **5**, 046002 (2010).
22. P. R. Bandyopadhyay, D. N. Beal and A. Menozzi, "Research article biorobotic insights into how animals swim," *J. Exp. Biol.* **211**, 206–214 (2008).